DISCLAIMER

This report was prepared as an account of work sponsored by an agency of the United States Government. Neither the United States Government nor any agency thereof, nor any of their employees, makes any warranty, express or implied, or assumes any legal liability or responsibility for the accuracy, completeness, or usefulness of any information, apparatus, product, or process disclosed, or represents that its use would not infringe privately owned rights. Reference herein to any specific commercial product, process, or service by trade name, trademark, manufacturer, or otherwise does not necessarily constitute or imply its endorsement, recommendation, or favoring by the United States Government or any agency thereof. The views and opinions of authors expressed herein do not necessarily state or reflect those of the United States Government or any agency thereof. Reference herein to any social initiative (including but not limited to Diversity, Equity, and Inclusion (DEI); Community Benefits Plans (CBP); Justice 40; etc.) is made by the Author independent of any current requirement by the United States Government and does not constitute or imply endorsement, recommendation, or support by the United States Government or any agency thereof.

ORNL/TM-2024/3646

Radiation Dose Modeling for Niowave's Accelerator-Driven Uranium Target Assembly 3

R. Blake Wilkerson
Chad Denbrock
Terry Grimm
Jim Nash
Jorge Navarro
Robert Wahlen

Approved for public release.
Distribution is unlimited.

December 2024

OAK RIDGE National Laboratory

ORNL IS MANAGED BY UT-BATTELLE LLC FOR THE US DEPARTMENT OF ENERGY

ORNL/TM-2024/3646

Nuclear Energy and Fuel Cycle Division

RADIATION DOSE MODELING FOR NIOWAVE'S ACCELERATOR-DRIVEN URANIUM TARGET ASSEMBLY 3

R. Blake Wilkerson[1]
Chad Denbrock[2]
Terry Grimm[2]
Jim Nash[1]
Jorge Navarro[1]
Robert Wahlen[2]

[1]Oak Ridge National Laboratory
[2]Niowave Inc.

December 4, 2024

Prepared by
OAK RIDGE NATIONAL LABORATORY
Oak Ridge, TN 37831
managed by
UT-BATTELLE LLC
for the
US DEPARTMENT OF ENERGY
under contract DE-AC05-00OR22725

CONTENTS

LIST OF FIGURES

LIST OF TABLES

LIST OF ABBREVIATIONS

ADVANTG	Automated Variance Reduction Generator
MAVRIC	Monaco with Automated Variance Reduction using Importance Calculations
MCNP	Monte Carlo N-Particle
ADSR	accelerator-driven subcritical reactor
CADIS	Consistent Adjoint-Driven Importance Sampling
FOM	figure of merit
FW-CADIS	Forward-Weighted Consistent Adjoint-Driven Importance Sampling
LBE	lead-bismuth eutectic
LEU	low-enriched uranium
MC	Monte Carlo
NNSA	National Nuclear Security Administration
ORNL	Oak Ridge National Laboratory
ROM	reduced-order model
SPSG	secondary particle source generator
TTB	thick-target bremsstrahlung
UTA	uranium target assembly

ACKNOWLEDGMENTS

This material is based upon work supported by the US Department of Energy, National Nuclear Security Administration, Office of Defense Nuclear Nonproliferation, Office of Material Management and Minimization, Molybdenum-99 program.

Special thanks are extended to Dr. Noel Nelson in the transition of shielding work from uranium target assembly (UTA)-2 to UTA-3 as well as valuable discussions on variance reduction methods for the Niowave UTA-3 facility.

ABSTRACT

Molybdenum-99 is a high-value radionuclide commonly used for medical purposes within the United States. The National Nuclear Security Administration (NNSA) seeks to reliably produce the radioisotope ^{99}Mo without the use of highly enriched uranium. NNSA's Office of Material Management and Minimization (M3) provides funding and government laboratory expertise to private companies to expedite the production process domestically and currently funds designs that use low-enriched uranium or other ^{99}Mo production pathways. Several production designs are being explored across the industry, including uranium fission and photonuclear conversion of ^{100}Mo targets. Niowave Inc. seeks to produce ^{99}Mo via a high-energy electron accelerator that strikes a lead-bismuth eutectic target that ultimately produces a consistent neutron flux. The neutron flux then interacts in a subcritical reactor core configuration to produce fission in low-enriched or natural uranium targets. These fissionable targets are then processed to extract ^{99}Mo. The purpose of this work is to estimate the neutron and photon dose response across Niowave's proposed facility for worker safety during operation. Owing to the size of the proposed Niowave facility and necessary shielding, unbiased Monte Carlo radiation transport is impractical, and variance reduction methods are required. This work focuses on the weight window variance reduction method to produce high-confidence dose response results within a Monte Carlo radiation transport code. Specifically, an adjoint-informed weight window methodology was created to improve the dose response estimates for accelerator-driven subcritical reactor designs. This adjoint-informed methodology was implemented for Niowave's proposed design and improved dose results at far-field locations across the facility. Acceptable dose rate contours for the proposed facility were generated across the facility and are presented in this work.

1. INTRODUCTION

The United States depends on a constant supply of ^{99}Mo for medical procedures. Molybdenum-99 decays into ^{99m}Tc, which is used for approximately 40,000 medical procedures each day and roughly 85% of all imaging across the globe [4]. The majority of ^{99}Mo is supplied by foreign partners in Australia, Belgium, the Netherlands, and South Africa. These partners have previously used highly enriched uranium for ^{99}Mo production but are converting to low-enriched uranium (LEU) or have already done so [4]. The National Nuclear Security Administration (NNSA) continues to work toward meeting ^{99}Mo demands by providing a program to support the establishment of domestic supplies of ^{99}Mo via various conversion methods. NNSA has funded several projects, including a feasible design with Niowave Inc. to produce ^{99}Mo via an accelerator-driven subcritical reactor (ADSR) assembly. Oak Ridge National Laboratory (ORNL) is jointly funded to provide expertise and tool-set capabilities to Niowave and other NNSA-funded designs for ^{99}Mo production.

NNSA leverages ORNL to provide expertise in advanced radiation transport capabilities to Niowave's ADSR design. The purpose of this work is to estimate the neutron and photon radiation doses for Niowave's proposed uranium target assembly (UTA) version 3, known as UTA-3. This analysis is built upon prior work performed by ORNL for Niowave's UTA-2 design in 2022 [8]. ORNL performed radiation shielding calculations for the UTA-2 design, including an initial reduced-order model (ROM) to convert a high-energy electron beam into a photon-neutron source [8]. The initial photon-neutron source was created for the `SCALE` suite [16], which is limited to such particles. `SCALE` was selected in the prior UTA-2 work because the radiation transport code Monaco with Automated Variance Reduction using Importance Calculations (`MAVRIC`) [9] contains both Consistent Adjoint-Driven Importance Sampling (CADIS) [14] and Forward-Weighted Consistent Adjoint-Driven Importance Sampling (FW-CADIS) [13] methods to perform deep-penetration shielding problems. Owing to the size and shielding of Niowave's UTA designs, the CADIS methods were considered viable choices for variance reduction.

This analysis uses both Monte Carlo N-Particle (`MCNP`) [11, 15, 10] and `SCALE` software to perform different parts of the transport analysis because `SCALE` cannot model the accelerator-driven electron beam source found in Niowave's ADSR design. `MCNP` is a highly capable radiation transport code that can transport not only neutrons and photons but also many other charged particles, and this physics is necessary for accelerator-driven systems.

This work involves reevaluating the ROM found in the prior UTA-2 analysis [8] and building upon that work by creating a set of weight window methods to vastly improve the statistics of a final `MCNP` transport calculation with full electron transport implemented. This work included modeling the full Niowave UTA-3 assembly, generating adjoint-informed weight windows, and simulating initial dose rates within the Niowave facility to expedite the shielding requirement for the facility.

1.1 NIOWAVE URANIUM TARGET ASSEMBLY 3

Niowave is one of several companies seeking to generate a substantial portion of the US and global demand for ^{99}Mo. Their design for ^{99}Mo production uses a high-powered electron accelerator that strikes a flowing lead-bismuth eutectic (LBE) producing high-energy bremsstrahlung radiation (>10 MeV). The LBE has a relatively low melting point, which makes it well suited to flow through a target region of the core. Because the material is constantly flowing (and externally cooled), the target material does not become overheated while the accelerator is active. Importantly, both bismuth (^{209}Bi) and lead (^{204}Pb, ^{206}Pb, ^{207}Pb, and ^{208}Pb) have significant photonuclear cross sections (Figure 1), making them good candidates for

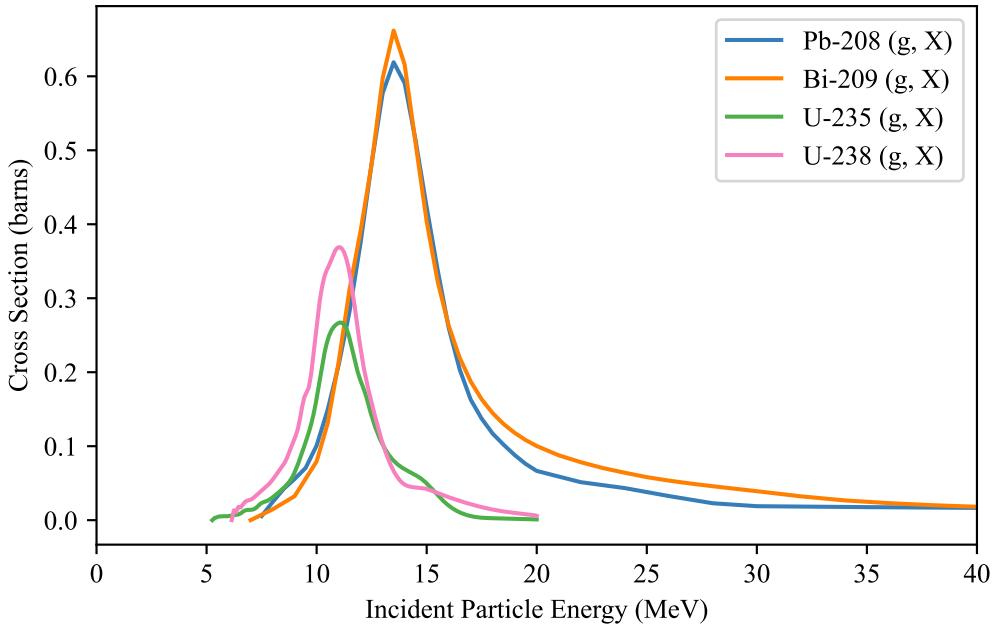

Figure 1. Photonuclear cross sections for four common isotopes in the Niowave ADSR. The photonuclear reaction cross sections exclude other separately tabulated reactions such as the uranium photofission cross sections shown in Figure 2. Lead (Pb) has three other naturally occurring isotopes that exhibit similar cross sections to those of the ^{208}Pb shown here.

photoneutron conversion from any high-energy bremsstrahlung. The photoneutrons are the main conversion channel to create the accelerator-dependent neutron flux in the UTA-3 core region.

The high-energy bremsstrahlung is intended to produce photoneutrons that cause subsequent fission in the subcritical reactor configuration. The UTA consists of both LEU and natural uranium U_3O_8 rods arranged around the two LBE targets. In addition to the photoneutron-induced fission, some high-energy photons also create photofissions in the two dominant isotopes of uranium, as shown in photofission cross sections of Figure 2. These are the main pathways for fission generation and thus ^{99}Mo production in the UTA-3 core.

The proposed UTA-3 facility (Figure 3) houses two high-powered electron accelerators along underground tunnels that are directed toward a UTA at the center of the facility (Figure 4). The subcritical reactor sits in a deep pool of water to moderate neutrons, remove core heat, and shield the facility.

The core vessel is lined with steel and wrapped in a thick layer of concrete for support and shielding. The LBE flow components are housed in two large ports. In the initial Niowave design, no additional shielding was provided at the port regions, although later work added significant shielding pieces just outside the LBE ports. The facility layout in Figure 3 shows the ground level across most of the facility. The accelerator tunnels are a few feet below ground level for shielding. Directly above the accelerator tunnels is several feet of fill sand, which provides additional shielding in the facility. Additional corridors run perpendicular to the accelerator tunnels. Both the accelerator tunnels and corridors had unobstructed paths to the main floor of the facility in the original design. However, based on an initial dose analysis, movable concrete doors were positioned in these openings during operation to attenuate both neutrons and gammas. Based on an iterative shielding analysis for the Niowave UTA-3 design, further additional shielding was added to the facility along the accelerator tunnels and above the reactor vessel.

The layout of the facility clearly indicated that particles would need to be transported large distances and

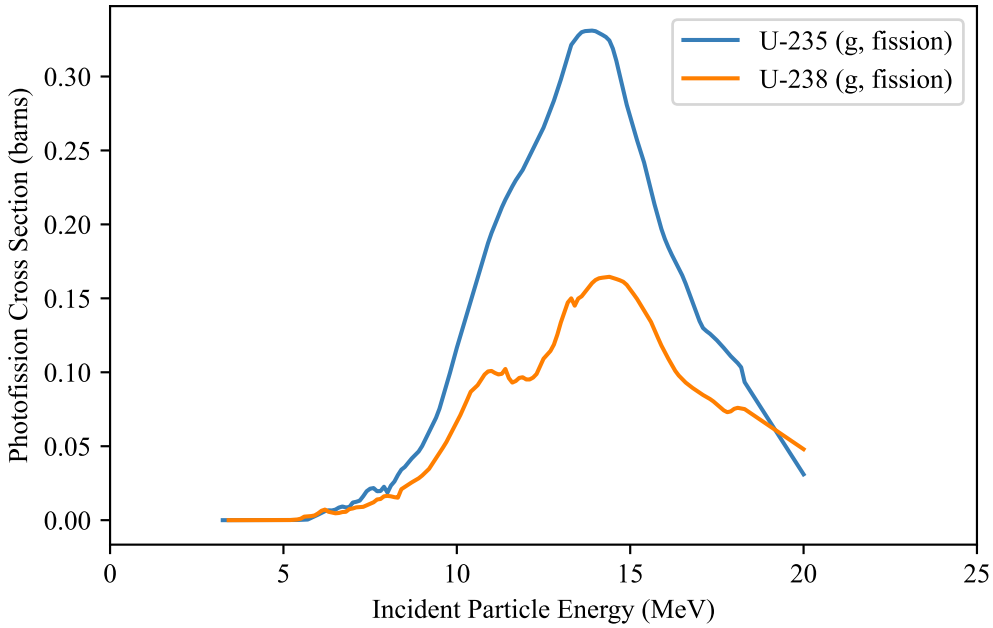

Figure 2. Photofission reaction cross sections for ^{235}U and ^{238}U.

interact in multiple shielding locations to reach regions of interest such as the facility floor, upper floor above tunnels, and walking corridors. Neutron activation of the facility, although not discussed in this work, shares many of the same requirements as a neutron dose rate, so any optimization of facility fluxes in a Monte Carlo (MC) transport was beneficial in several areas of radiation shielding. Additionally, because some bremsstrahlungwas above 5 MeV, a pathway existed for photon activation, which fortified the need for accurate neutron and photon fluxes across the facility.

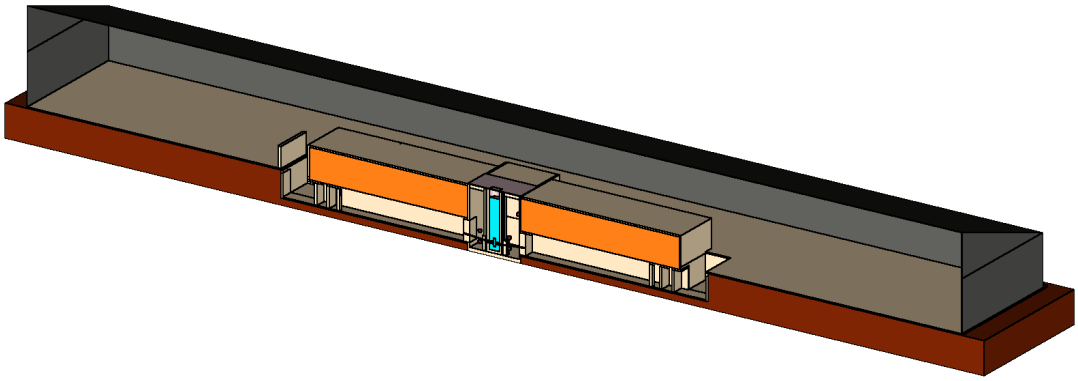

Figure 3. View along the accelerator tunnels of Niowave's UTA-3 facility.

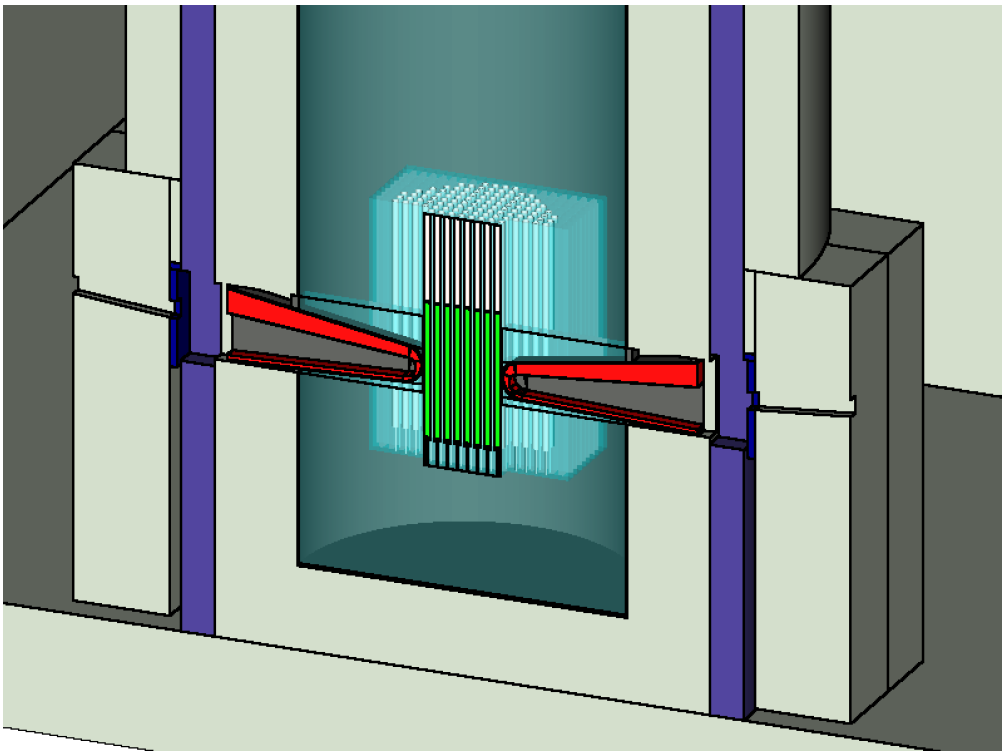

Figure 4. Niowave's proposed UTA-3 core geometry. Two electron accelerators hit the LBE (red) to convert electrons into photoneutrons. Additional shielding was added near the electron beam ports to reduce dose rates in the vessel room and accelerator tunnels.

2. ADJOINT-INFORMED WEIGHT WINDOW GENERATION

The two main goals of this work scope were to understand (1) dose rates and (2) activation levels of facility components. Both goals require accurate neutron and photon fluxes at the facility. Without a high confidence level in these fluxes, the dose and activation results are highly uncertain, leading to poorly designed facilities that have excessive costs, dose rates, or both.

For some radiation transport scenarios, the necessary neutron and photon fluxes are easily attainable with minimal variance reduction in MC transport codes. The Niowave-specific ADSR was a far-field, deep-penetration problem with particle fluxes many orders of magnitude lower than the in-core levels. Because it was a deep-penetration problem, variance reduction was a necessary addition to the MC transport to generate accurate fluxes outside the reactor core area. Optimal variance reduction methods for ADSR designs were unclear, with little to no published research on the matter. Recent work using accelerators and fission systems has largely been at low power, which is less likely to produce a high radiation dose response. This work explored automated weight window generators for the variance reduction in the Niowave facility.

Weight windows are one of several variance reduction methods for MC transport. In MC transport tools, each source particle starts with a weight value. In analog transport, the particle weight is kept constant. Some variance reduction methods will artificially bias the outcome of certain reactions, but to prevent biasing the final result, will adjust the resulting particle weights. Weight windows operate on this concept. The goal of MC weight windows is to move particle weights toward "target weights" during transport. Target weights are any weight within the bounds of a weight window. MC weight windows have a lower and upper boundary for particle weights. If a MC particle weight is below the lower weight bound, Russian roulette is performed and the particle's weight is either increased after roulette survival or the particle is killed. Conversely, if the particle weight is above the upper weight window bound, the simulated particle is split into a subset of identical particles with weights inside the bounds of the weight window. Typically, weight windows are created to increase the number of particles as they move toward a region of interest and roulette particles as they move away from an important region. More discussion on weight windows is provided in the `MCNP` manual [11]. User-defined weight window generation can be time intensive and poorly optimized, causing minimal transport improvements or erroneous results. In this context, automated weight windows are a desirable option for both the user's time and solution accuracy.

For a tally region of interest, automated weight window generation has been implemented in `MCNP` for decades [1]. The challenge for this method involves transferring particles to the location(s) of interest. For example, in the UTA-3 facility layout, an analog transport may not register a tally score after several hours on a high-performance computing machine. The automated generator with `MCNP` would not appropriately update the weight windows in `MCNP` without a tally response. A common work-around for the `MCNP` weight window generator involves adjusting material densities and iterating back toward the true transport scenario, but this is also user intensive, particularly if the user must switch to another region of tally optimization within the model. In light of the user-intensive `MCNP` weight window generator within the Niowave-specific ADSR, a deterministic CADIS solution was selected to create a set of weight windows based on documented use cases for both the `MAVRIC` [9] and Automated Variance Reduction Generator (`ADVANTG`) [7, 5] codes. Both of those codes use `SCALE`'s `Denovo` discrete ordinates code [3], and each code has FW-CADIS to optimize multiple tally regions in the same transport solution. The Niowave facility required dose rate information at many locations, making the FW-CADIS methodology a useful option for an all-in-one simulation.

It became clear during this work that current physics and cross-section models of CADIS-based tools were not naturally suited to the Niowave ADSR design. The combination of an anisotropic bremsstrahlung

source, photonuclear particle production, and notable fission production created a daunting challenge for a discrete ordinates code to adequately capture the importance of each source and its impact on the final dose response across the facility.

The discrete ordinates code Denovo is limited to neutron and photon transport only, so the electron beam was converted into a usable combination of secondary source particles. This source complication was part of the reason that ORNL created the initial ROM for UTA-2 [8], which made a photon-neutron source from the original electron source. This work builds upon the original ROM methodology by creating a new set of scripts that together build MCNP and SCALE source definitions from the original MCNP electron transport.

2.1 SECONDARY SOURCE PARTICLE GENERATOR

The work performed by Nelson [8] for UTA-2 analysis began the process of converting the electron-photon-neutron problem into a reduced-order photon-neutron problem. This prior methodology relied on MCNP tallies surrounding the electron converter material, typically LBE. A reduced-order source was created from these tallies using the exiting photon and neutron energies along with pertinent angular information on the highly anisotropic source. The biggest challenge with tallying particle location, direction, and energy exiting a region of interest was how to properly define such a tally. Then, if created, remaking a complex surface source onto the geometry may prove difficult in any complex option. For example, the design of the UTA-3 LBE was a complex flowing shape. The radiation transport models used a set of quadratic surfaces to build the equivalent MCNP or SCALE cell. Determining optimal angles relative to the normal of a quadratic surface would be a complex task and ultimately difficult to handle. Similar approaches such as the surface source write feature of MCNP were not available in ADVANTG or MAVRIC. This work took a slightly different approach by grabbing the secondary particles at their inception and not the outward surfaces of the target converter regions. The initial source location methodology has an inherent advantage: it can be easily formed into a volumetric source for CADIS-based codes such as ADVANTG or MAVRIC.

MCNP's PTRAC module can print all the necessary particle information from a transport calculation, including the starting position, energy, and angle of particles at their genesis. A new, simple set of scripts called the secondary particle source generator (SPSG) ran MCNP's PTRAC with the accelerator-driven model. The SPSG scripts imported the PTRAC information and binned the secondary particles (bremsstrahlung photons and photoneutrons) into a set of position-, energy-, and angle-dependent bins to capture the source term for an ADVANTG or MAVRIC run. The SPSG scripts were built for the electron transport in Niowave's design, but this method could be applied to other complex radiation physics or other charged particles that MCNP can transport. The PTRAC method was a good option for secondary sources, but a few hindrances to its widespread usage exist. First, in MCNP versions before MCNP-6.3.0, the PTRAC module needed to run in serial mode. This creates a problem in sufficiently sampling the accelerator source and converting it into a generally accurate secondary source. This work ran multiple MCNP inputs with different random number seeds to work around this limitation, but multiple files needed to be processed to generate the secondary particle source. During the MCNP simulation, every electron accelerated into the Niowave LBE target created tens of primary bremsstrahlung photons (i.e., bremsstrahlung produced from the source electrons, not from secondary photoelectrons) at varying energies. Particle information for millions to billions of particles greatly inflated the resulting PTRAC output file size. This work produced multiple files well above 4 GB each, which also slowed the process time to extract the information. A more integrated MCNP tally might solve the PTRAC issue in the future, although it is unclear how MCNP could accomplish such a task internally without new tally filters.

The most user-intensive portion of the SPSG method was the discretization of the lead-bismuth photon-neutron source into an appropriate ROM source. The PTRAC output was a set of distinct bremsstrahlung

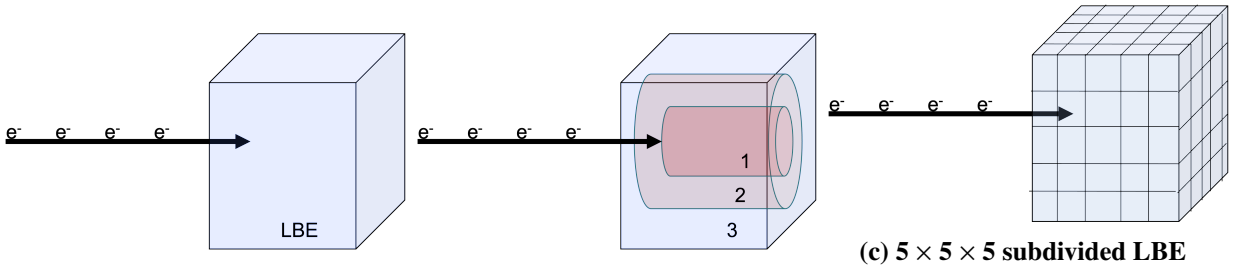

(a) 1 undivided LBE region **(b) 3 custom cell LBE regions** **(c) 5 × 5 × 5 subdivided LBE regions**

Figure 5. LBE converter in UTA-2 divided into three options for regions.

and photonuclear particles with different energies, angles, and source positions. To easily integrate the source into ADVANTG or MAVRIC, the secondary neutron and photon sources needed to be binned (i.e., tallied) by energy, angle, and position to generate an appropriate source for Denovo. To evaluate the SPSG scripts, the UTA-2 simplified LBE cuboid was evaluated to determine how effective the secondary source generation was relative to the benchmark electron beam. Figure 5a is a rough rendering of the UTA-2 cuboid and the impinging electron pencil beam. Several configurations were tested to evaluate the secondary particle source relative to the benchmark electron beam source. Figure 5 shows three of four configurations evaluated for the SPSG to electron beam comparison.

The first configuration (Figure 5a) sampled source particles uniformly in a singular region. It mimicked a scenario in which bremsstrahlung and photoneutrons would be "birthed" uniformly in the cuboid region. The three-cell configuration (Figure 5b) split the LBE cuboid into three distinct cells for the MCNP PTRAC run. The SPSG scripts filtered the PTRAC output by cell and generated cell-specific sources. The third configuration (Figure 5c) used the first LBE cuboid data, so the MCNP deck did not need to be manipulated, which was advantageous. The $5 \times 5 \times 5$ grid was a postprocessing discretization overlapping the LBE region. If a particle in the PTRAC output file started inside a $5 \times 5 \times 5$ grid voxel, it was tallied in this region for energy and angle. The grid overlay was similar to cell filtering without the need to build new MCNP cells. An additional set of six concentric cylinders, which were similar to the three cylinders of Figure 5b, was the final configuration. These configurations evaluated the position of the source sampling and its impact on the final result. Figures 6 and 7 plot the outgoing energy of neutrons and photons from the surface of the LBE.

MCNP-5.1.60 cannot handle multicell rejection, so the option for a multicell SPSG method was fine for scoping calculations, but it was not selected during the full-scale UTA-3 modeling. The SPSG results behaved as expected; finer position discretization (i.e., 5× grid, 6 cylinders) improved the exiting neutron and photon spectra.

For neutrons, the starting position had a small effect on the final neutrons leaving the LBE. This result suggested neutrons were largely unaffected by source position in the LBE material. The highest-energy bins varied in exit intensity, but this was likely due to uncertainties in the sampling frequency above 20 MeV. The highest fraction of photoneutrons was well aligned among all configurations to the electron benchmark analysis. The summation of all photoneutrons exiting the LBE for the SPSG photoneutron sources was 2% off the benchmark electron beam. The systematically higher SPSG neutrons per electron results from the LBE were surprising given that each SPSG source amounted to 0.0085 neutrons per source electron, with little variation.

Although not applicable to this specific grid, the SPSG tool will automatically remove voxels with zero source tallies from the final MCNP or MAVRIC source generator. Additionally, the grid voxel sources can still use a single-cell rejection within MCNP-5, which means a complex shape can be discretized into fixed bins,

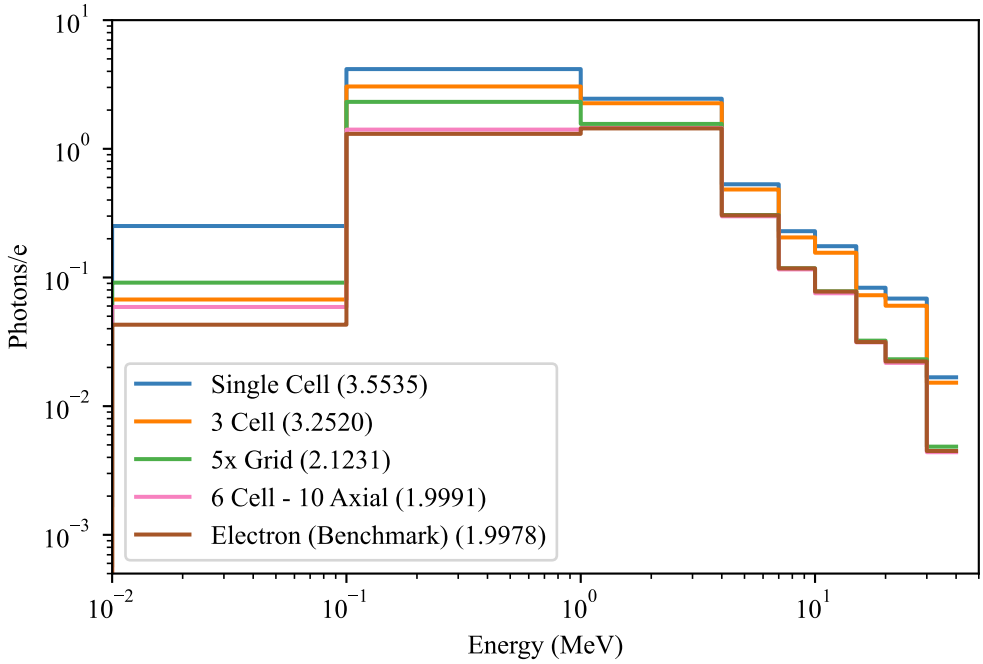

Figure 6. Photon particle emission rates per electron from UTA-2 LBE model. Summation of all photons/e above 1 MeV is shown in the legend for each SPSG method.

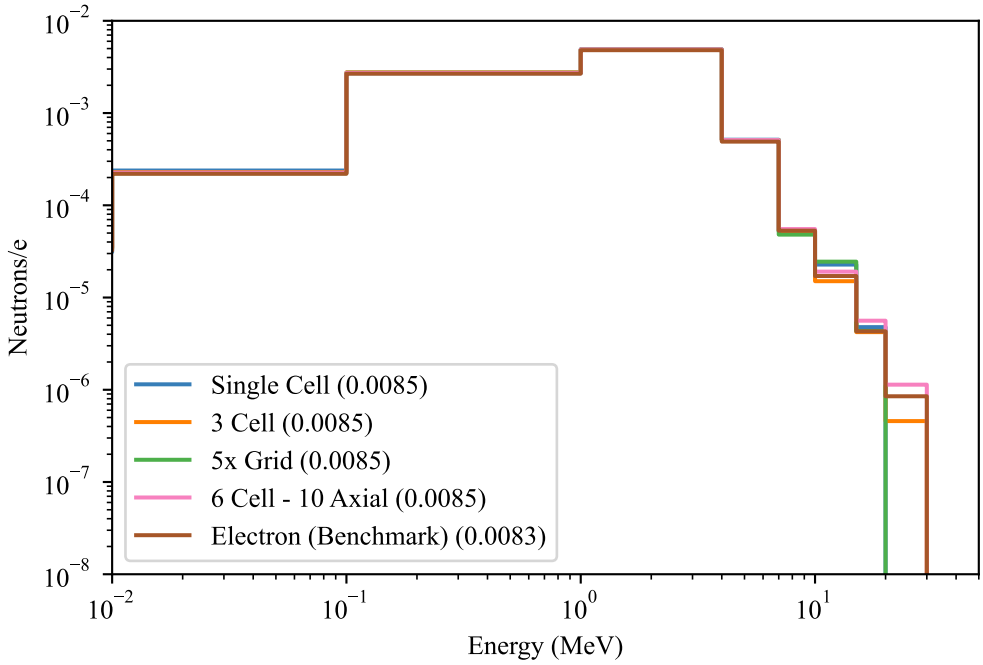

Figure 7. Neutron particle emission rates per electron from UTA-2 LBE model. Summation of all neutrons/e is shown in the legend for each SPSG method.

but `MCNP` can properly reject on a uniquely shaped source. This was ultimately the preferred choice for this analysis: custom Cartesian bins around the LBE source area that reject on the LBE source cell and/or material. In the UTA-3 design, breaking down the source LBE into subcells would be time-consuming for the user without a considerable benefit.

2.1.1 UTA-3 Lead-Bismuth Eutectic Conversion Target

The UTA-2 LBE conversion was a simple rectangular prism with an incident 20 MeV electron beam. UTA-3 increased the energy of the electrons to 40 MeV and further increased the electron production rate (i.e. beam power). To dissipate heat effectively, the LBE needed to continually flow within a core region such that the electron beam was not overheating the LBE. The Niowave design is a complex quadratic surface definition mimicking the flow of LBE. A rendering of the eutectic is shown in Figure 8. The SPSG tool was implemented for the UTA-3 LBE using a custom 3D grid and cell rejection. The SPSG code suite was also improved to handle custom source angles for both `MCNP` and `SCALE` sources. Once the UTA-3 core design was largely set, the SPSG source definitions for both `MCNP` and `SCALE` remained constant. Initially, the SPSG scripts had to rebin particles above 20 MeV into the lower-energy bins because the multigroup libraries of `SCALE` had no bins above 20 MeV. During this work, `SCALE` developers created a custom photonuclear multigroup library with energy bins up to 200 MeV for neutrons and photons, thereby enabling the full SPSG source definitions to be run in `MAVRIC` for adjoint deterministic transport calculations.

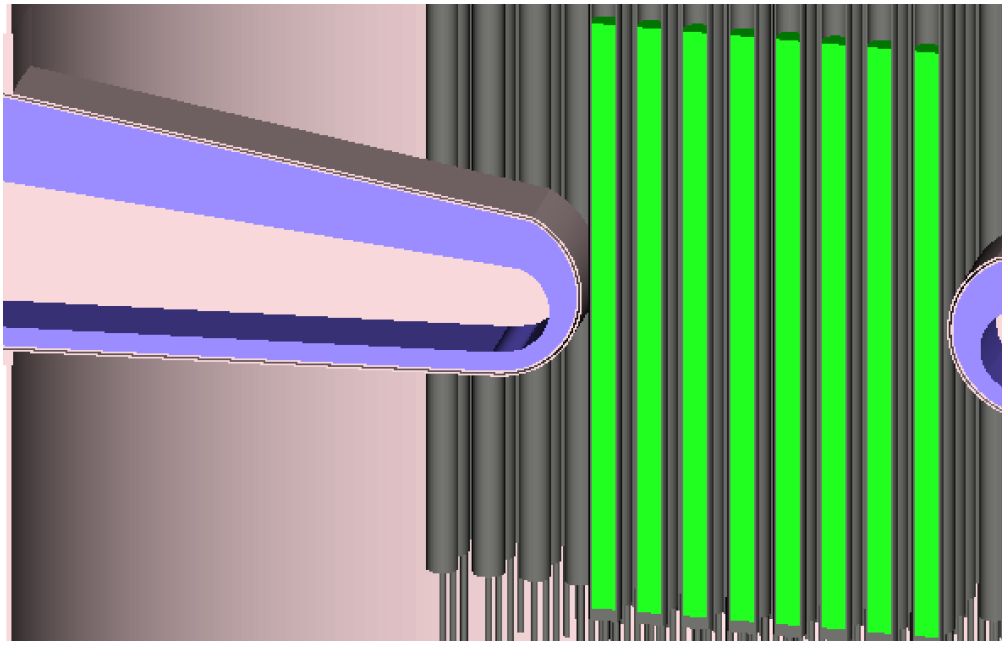

Figure 8. SCALE rendering of Niowave's LBE target (purple).

The SPSG tool set was used to create a bremsstrahlung and photoneutron source from the primary electron source. It was quickly determined that photoneutrons were a simple extraction from the `PTRAC` file, but bremsstrahlung was more complicated. It was desirable to build a bremsstrahlung source but not the full set of bremsstrahlung produced in the LBE. If every possible bremsstrahlung particle was accounted for, the photonuclear physics and thick-target bremsstrahlung (TTB) models would have to be preferentially turned off in source cells of the MC transport to prevent double production in the final transport. The primary bremsstrahlung (i.e., bremsstrahlung directly produced from the original beam of electrons, not secondary electrons created from other bremsstrahlung) was needed for a ROM source. With only primary bremsstrahlung, the LBE regions could still use full particle physics. Therefore, the `MCNP PTRAC` models were manipulated in such a way that only primary bremsstrahlung would be printed to the `PTRAC` file alongside photonuclear interactions. Both bremsstrahlung and photoneutrons were extracted from `PTRAC` files and made into functional source definitions for both `MCNP` and `SCALE`. For consistency across codes, the energy binning and position discretization were limited due to `MCNP`'s 1,000 distribution restriction in a fixed-source problem.

Even with a functional neutron-photon source, analog transport was insufficient, which is discussed in Section 3. The creation of a reduced-order source was beneficial not only for using SCALE MC transport but also for using CADIS methods for dose shielding. CADIS methods have proven beneficial in many MC transport cases. For this work, CADIS methods were used to generate the initial weight windows for both SCALE and MCNP transport.

2.2 CADIS-BASED WEIGHT WINDOW GENERATION FOR THE ADSR

The theory and application of CADIS-based variance reduction methods are not discussed in this report, but numerous references for ORNL's work [9, 14, 12, 13, 7] provide both theory and application of the methodology. From an application level, CADIS and FW-CADIS both provide a set of weight windows and typically source biasing in fixed-source problems. This work used SCALE's MAVRIC sequence because it allowed more sources of both neutrons and photons compared with ADVANTG. In addition to the SPSG photoneutron and bremsstrahlung source capability, a fission source can be easily generated and implemented within the SCALE suite. ADVANTG was not updated to the beta capabilities of SCALE-7.0 like the high-energy multigroup library. For the Niowave UTA-3 design, the biggest challenge was creating reasonable forward transport sources (i.e., bremsstrahlung, photoneutrons, and prompt neutrons and photons from fission) and adjoint sources (i.e. regions of interest or optimized tally locations). These are briefly discussed in the context of the Niowave ADSR design.

2.2.1 Reduced-Order Radiation Sources

In an ideal scenario, CADIS tools would be able to simulate electron transport such that simple electron source definitions could be used in tools such as ADVANTG and MAVRIC. Although MCNP can handle such a source, no CADIS-based tool, as of yet, can simulate more than neutrons and photons. The SPSG method was arguably sufficient for generating a ROM bremsstrahlung source. However, if a bremsstrahlung source was simulated for the Niowave core assembly, neutron flux was zero. This was because there was no photonuclear physics production in Denovo. To alleviate this source insufficiency, a photoneutron source was extracted from the PTRAC file alongside the bremsstrahlung source. Even with a photoneutron source, the neutron source definition was incomplete in Denovo because fission, a considerable multiplier in ADSR designs, was treated as absorption only, not a production pathway. This lack of fission production causes a major issue in the core of the Niowave design. To capture the fission physics, SCALE's KENO sequence has a well-defined method to generate a fission mesh neutron source definition that was imported for fixed transport in Denovo. Although not ideal, using a bremsstrahlung, photoneutron, and neutron fission source in Denovo produced somewhat reasonable weight windows, particularly outside the core region.

2.2.2 Adjoint Sources or Regions of Interest

FW-CADIS methods use a set of regions to optimize within a problem, which was vital for the Niowave design because both neutron and photon dose rates were needed across the facility. These optimization regions are equivalent to adjoint sources in an adjoint transport calculation. Selection of these adjoint sources was relatively straightforward depending on the problem. For the Niowave facility, certain regions were particularly important. The area just outside the tunnels and the area above the ADSR vessel were deemed important because both areas could potentially require personnel during operation. Figure 9 shows the location of the adjoint sources in this scenario with red boxes.

Figure 9 shows the MAVRIC importance map for a single neutron energy group for the UTA-3 facility. The importance map is a set of mesh-based target weights created from the Denovo adjoint calculation. In this neutron example, the importance map progressively shifted the neutron target weights toward lower values (blue, purple, and pink) starting from regions of higher target weights (orange, red) such as the core region. For MC transport, the importance map values are converted to weight windows using a user-defined

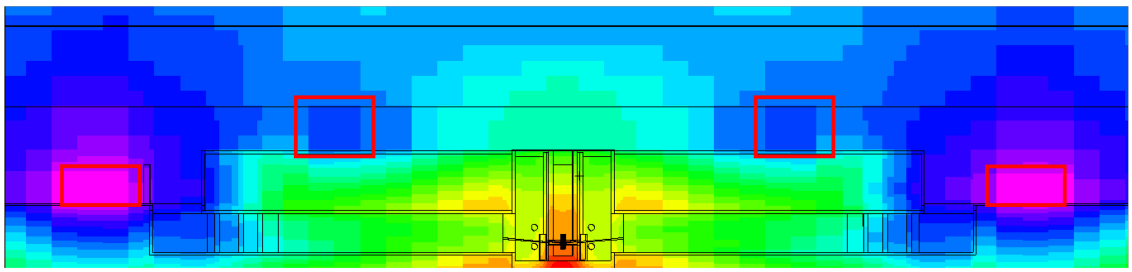

Figure 9. MAVRIC importance map for a single neutron group in Niowave facility. Four adjoint source locations are depicted with red blocks. Pink and dark blue indicate regions of higher importance for the final transport.

window ratio. Lowering the target weight as particles transported toward regions of interest would split particles to fit within the weight window bounds of a mesh voxel. This splitting caused more lower-weight particles to score in tally regions of interest. Conversely, as particles moved away from the important regions (e.g., into the ground), the target weights increased, which caused rouletting to occur as the particles attempted to increase their weight. As shown in Section 3, these adjoint source selections produced excellent results where analog transport was insufficient.

2.2.3 Challenges for ADSR Models with CADIS Methods

For an ADSR, four main issues with the fixed-source deterministic transport problem were identified:

- There was no photonuclear production cross-section channel
- There was no charged particle physics
- The anisotropic bremsstrahlung source was treated as isotropic
- There was no fission production term in the fixed-source calculation, only absorption

The lack of charged particles and photonuclear production channel was alleviated by the SPSG sources of both bremsstrahlung and photoneutrons. The isotropic treatment of the anisotropic bremsstrahlung source could not be directly alleviated. For Denovo deterministic transport, fission was considered an absorption-only reaction (i.e., no further production of neutrons or photons). This physics difference has largely been avoided in most MAVRIC reactor transport calculations by generating a representative fission source for the fixed-source transport calculation and turning fission neutrons "off" in the final forward MC transport calculation; the fission particles were converted to a fixed source and no longer a production pathway. The problem with this assumption is that it works for a critical reactor but not necessarily a subcritical one, such as the ADSR. In a subcritical assembly, the fission distribution is not guaranteed to match the critical fission distribution estimated with k-eigenvalue codes such as KENO or MCNP's KCODE. The actual source of fission neutrons might be much closer to the LBE material than a critical scenario, for example.

In light of the challenges in making a true neutral particle source definition for MC and deterministic transport, the final MC transport for this work reverted to the original electron beam and turned on all physics to remove any ROM source issues in the final dose rates. Because fission production was turned on in the final transport, the adjoint produced an unfavorable result in the reactor core region. Figure 10a shows an unwanted outcome for a group of thermal neutrons in the core. As discussed, the core used a fixed fission neutron source for the adjoint solution because photoneutrons were only absorbed in the core. They did not have a true production cross section like, for example, the (n, γ) production cross section. Because there was no production, thermal neutrons in the core had a very low importance relative to the fast neutrons. Theoretically, a thermal neutron has a high likelihood of fissioning and producing higher-energy neutrons

and photons. Normally, this should give a thermal neutron in the core a higher importance to fully sample the source, but in the actual Denovo transport, it was unimportant due to the absorption assumption. An issue occurs when running full electron physics in MCNP with CADIS-generated weight windows, and fission production was almost nonexistent when using unaltered weight windows. This issue can be potentially alleviated by adding an adjoint source in the fuel to boost the importance of the fissioning material or manipulating the weight windows in postprocessing. This was where "Frankenstein" weight window manipulator scripts were applied to the Niowave UTA-3 model (see Section 2.3)

2.3 FRANKENSTEIN WEIGHT WINDOW MANIPULATOR

At the beginning of the ADSR work, it became clear that the CADIS-based methods would be effective for variance reduction. The main issue was determining how to create an effective set of neutron and photon weight windows. Two concurrent paths were evaluated for building a set of weight windows for transport: ADVANTG and SCALE's MAVRIC sequence. In the beginning of the shielding analysis, ADVANTG was a natural option because Niowave had started with an MCNP model of the UTA-2 and UTA-3 designs. Once the analysis began, the limitations of ADVANTG for secondary particle sources became clear. As discussed, the SPSG created both bremsstrahlung and photoneutron sources, as needed for the user. ADVANTG-3.2.0 was limited because it required source definitions as defined by MCNP-5.1.60 [11]. MCNP-5.1.60 can only simulate one particle type in the SDEF card at a time. This limitation directly impacted the Niowave ADSR design. During this work, the Denovo discrete ordinates code had no photonuclear cross sections to produce neutrons, so an all-in-one ADVANTG run would be missing all neutron transport. For full physics, this work produced two different sources: bremsstrahlung for one ADVANTG simulation and photoneutrons for another ADVANTG simulation. These separate runs produced the photon and neutron weight windows for the final transport calculation, but because there were two ADVANTG runs, they needed to be melded into one set of weight windows for the final transport in MCNP. A set of Python scripts was built to import data from multiple weight window input files and produce a Frankenstein combination of the two. From this melding feature, additional adjustment capabilities were added to the Frankenstein scripts to adjust the weight windows of a CADIS solution. Because Frankenstein edited and merged data from multiple CADIS-based importance maps, the final weight window sets were adjoint-informed but not fully based on the original importance maps from ADVANTG or MAVRIC. Because ADVANTG was not selected for producing weight windows, Frankenstein scripts were only used for weight window manipulation in the reactor core region (Figure 10) and for removal of extraneous weight window energy bins. By removing some energy-dependent weight windows, Frankenstein reduced the weight window file sizes considerably, and MCNP forward transport spent less time evaluating particles for splitting or roulette. The Frankenstein weight window manipulation in the core allowed thermal neutrons (Figure 10c) to remain alive long enough to generate fission neutrons and photons.

2.4 NIOWAVE FACILITY DESIGN

Most of the Niowave facility design challenges fell within the core region (source location, source shape, source type, etc.). The Niowave facility built around the vessel was relatively straightforward. There were accelerator tunnels just below the ground level and walkways down into the vault region. The Niowave design, as modeled, had ports for the LBE to flow into the core region, but the remainder of the core vessel was sealed with steel and concrete except the top steel port to access the pool water. The MCNP facility models were built to general specifications from Niowave, but additional shielding was required based on initial dose rates. The tunnel and port shielding (Figures 3 and 4) were selected based on multiple dose rate calculations at the facility. Model iterations involving labyrinth walls along tunnels, full tunnel shields, and additional concrete walls were all considered in this work to reduce dose rates. Dose rates were most improved by adding additional iron and concrete vessel shielding along the full length of the vessel. Substantial tungsten carbide sheets were affixed to concrete shields at the exit of each LBE port region. This was

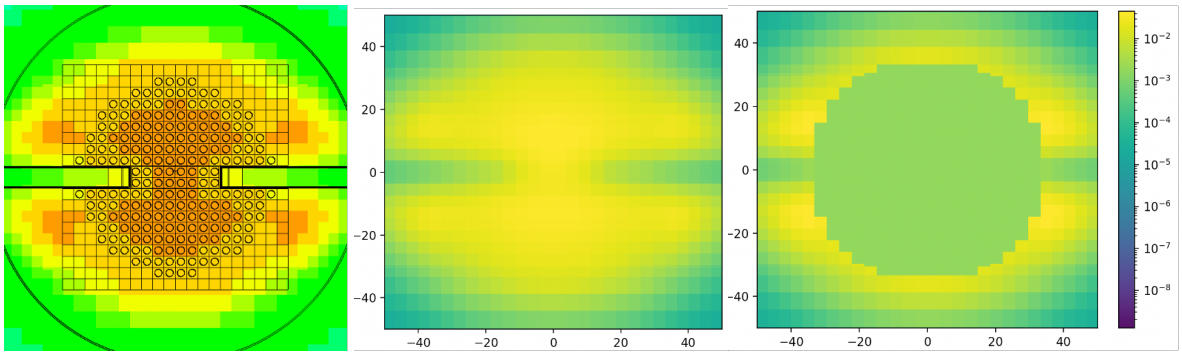

(a) UTA-3 reference with uranium targets **(b) FW-CADIS lower-weight window bounds** **(c) Weight window manipulation with Frankenstein**

Figure 10. Frankenstein weight window manipulation of UTA-3 core region for thermal neutrons.

essential largely due to the substantial photon and neutron flux emitted from the LBE ports. The increased shielding dropped dose rates to levels in line with Niowave expectations during operation.

One of the main challenges was creating a copy of the geometry for both `MCNP` and `SCALE`. The codes use different input syntax for arrays of materials like the reactor core rods. `SCALE` has unique "hole" features that can greatly improve transport run times, a feature not present in `MCNP`. A notable difference was the lack of a union operator while building an equivalent LBE geometry in `SCALE` from the initial UTA-3 `MCNP` model. The `SCALE` LBE was modeled as multiple regions without the union operator. At the same time, `SCALE` holes allowed for the same LBE geometry to be easily mirrored in the opposite direction.

Editing two different input files for the variance reduction techniques made this problem user-intensive. Although the feature is not explored in this work, `SCALE` has an interface for using `MCNP` geometry similar to that of the methods employed by `ADVANTG`. `ADVANTG` only allowed the source definition as defined in the `MCNP` input file. It is conceivable that the SPSG source definitions could be defined outside the `MCNP` input such that both photons and neutrons could be modeled via `Denovo`. Even still, this leaves an unclear path for creating a fission source term via an `MCNP` file. `SCALE`'s natural ability to use SPSG sources and easily generate a fission source made it a natural choice for the `Denovo` adjoint deterministic transport.

3. NIOWAVE URANIUM TARGET FACILITY DOSE RESULTS

Niowave originally generated the UTA-3 core design using MCNP with two opposite-firing 40 MeV electron beams at 200 kW each. The power level became the source particle normalization constant used for dose rate contours at the facility. If the facility scaled power up or down, the dose rates would change in proportion. The shielding and design team built a proposed facility around the core with model tweaks within the core for simplicity. Initial testing on the facility design used analog transport to confirm the model was correctly working. It became clear that facility dose rates were impractical via this method. Niowave required dose rates at many locations outside the core vault region (i.e., where workers might actively walk or worker stations). As shown in Figures 11 and 12, the analog transport produced very few particles outside the core vault regions. Longer analog MC calculations would require many weeks of transport to start producing dose rates outside the core, so variance reduction was required.

After the Frankenstein weight window manipulator is run on the SCALE-based weight windows, the original problem can be rerun using MCNP electron transport with neutron-photon weight windows. The weight window parameters were added to the MCNP input deck at this point. The weight window parameters were not automatically determined for this work. Iterative analysis was performed on different weight window ratios, splitting and roulette parameters, and scalar multipliers for the weight windows via the WWP card in MCNP. This portion required user intervention to ensure that the splitting did not become overly burdensome per source particle. Conversely, setting the weight window bounds to accidentally roulette important particles should be avoided. Excessive splitting led to a never-ending problem, and too many roulettes produced erroneous, poorly sampled results. In this work, many initial tests required hours of MCNP analysis for running a single high-energy particle history due to splitting issues. Because the adjoint-informed weight windows were imperfect for the ADSR, this work typically set the maximum number of particle splits to 10 per particle to limit the MC transport spent on a large number of low-weight particles. Additionally, window ratios normally exceeded 50 for both neutron and photon weight windows. The ratios were set above the default value (5) to avoid inappropriate particle splitting and roulette in the core region. Both the number of splits and the window ratios were not well-defined parameters for an ADSR and should not be considered well established in this work. For this work, equivalent analog simulation tallies

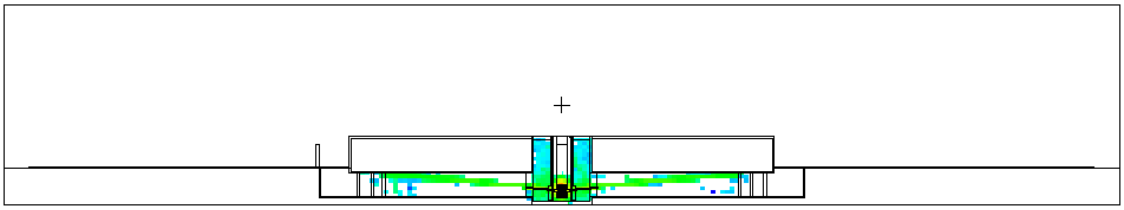

(a) MCNP analog transport with photonuclear collision biasing

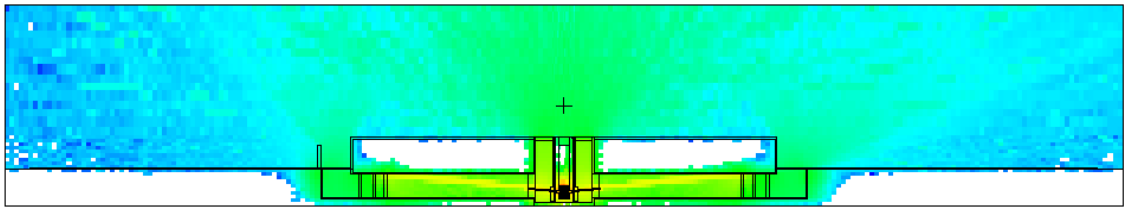

(b) Frankenstein weight window neutron dose rates without photonuclear collision biasing

Figure 11. A 2D slice of UTA-3 facility neutron dose rates. There are very few neutron tracks with analog transport outside the tunnels of the UTA-3 facility.

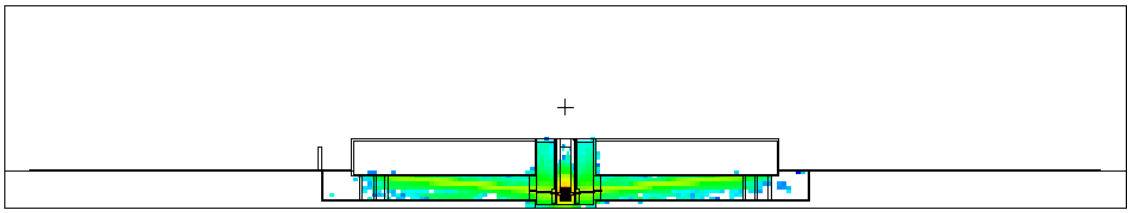

(a) MCNP analog transport with photonuclear collision biasing

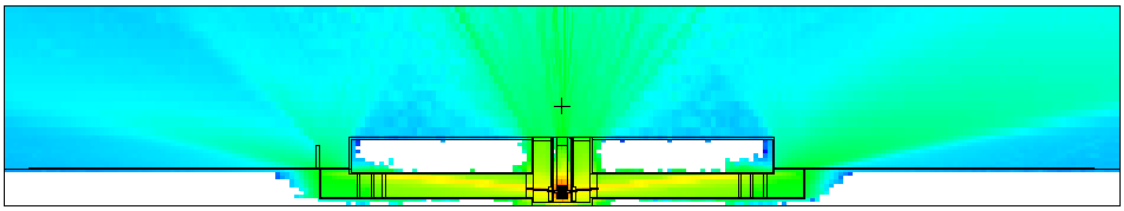

(b) Frankenstein weight window photon dose rates without photonuclear collision biasing

Figure 12. A 2D slice of UTA-3 facility photon dose rates. The results indicate more particle tracks outside the tunnels of the facility and on the main working floor of a Niowave UTA-3 facility.

were computed to confirm matching answers at low-variance regions to confirm rouletting was not inappropriately biasing the source. Even with adjustments to weight window ratios, splitting limits, and window normalization constants, the transport speedup was still noticeably improved versus the analog transport. The visual depiction of the dose rate maps in MCNP clearly indicated the weight window effectiveness. Figures 11 and 12 show the improvement for neutron and photon dose rates, respectively. The problems still needed substantial compute resources to run, however, particularly when good statistics were required outside the facility tunnels (e.g., radiation protection dose rate contours).

Figure 13 shows a horizontal cut plane through the facility accelerator tunnels, indicating the expected dose rates within the accelerator tunnels and walkways. Workers were not expected within these areas during operation, but these values were a good indicator for radiation streaming pathways and the general effectiveness of the shielding. If neutron fluxes were requested, dose response functions were removed from the mesh tallies to estimate neutron fluxes for neutron activation of the facility and equipment.

Niowave wanted to know where the dose rates exceeded regulatory limits during operation. The limits, as specified by Niowave, were typically 2–5 mrem·h^{-1} for workers at the facility. Mesh tallies across the facility were simulated to produce dose rate contours in the VisIt software [2] alongside a 3D representation of the Niowave facility. Dose rate contours were created to start an iterative discussion with Niowave on shielding at the facility. One of the initial iterations is shown in Figure 14, which indicated higher dose rate contours than the limits and, importantly, where the limits were exceeded. As shown in Figure 14, the area above the facility exceeded many of the limits, including a substantial 100 mrem·h^{-1} contour coming out just above the top steel cover of the reactor vessel. More worrisome were the side walkways at ground level that had 100 mrem·h^{-1} contours. The concrete wall at the end of the accelerator tunnel suppressed much of the photon dose rate seen streaming from the opposing accelerator tunnel that did not have a concrete wall. These results indicated that additional concrete or shielding materials would be needed along hallways and potentially right below the steel cover plate.

The final dose rate contours were in much better agreement with regulatory limits. Additional concrete shielding was placed at each doorway and at the end of each accelerator tunnel. These shielding pieces closed off the remaining streaming paths. The dose rate contours are shown in Figure 15. They indicate that photon and neutron dose rates were largely below 5 mrem·h^{-1} across the facility floor and above the

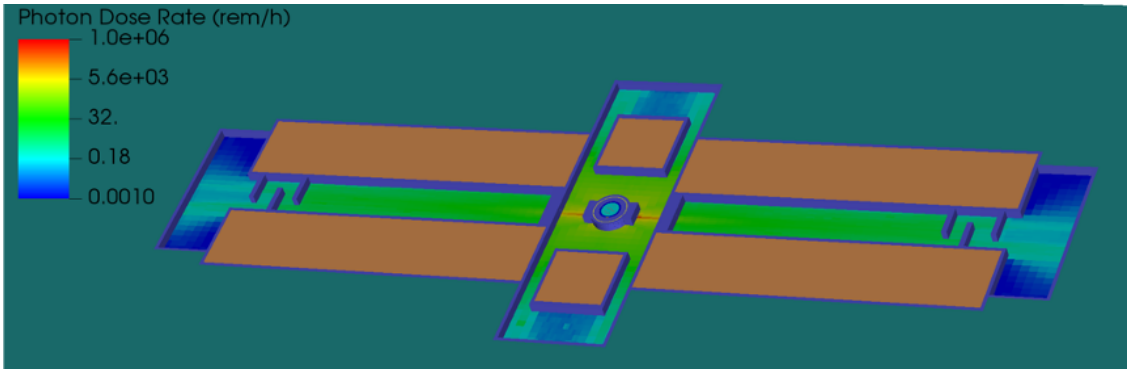

(a) Facility photon dose rates along accelerator tunnels and walkways

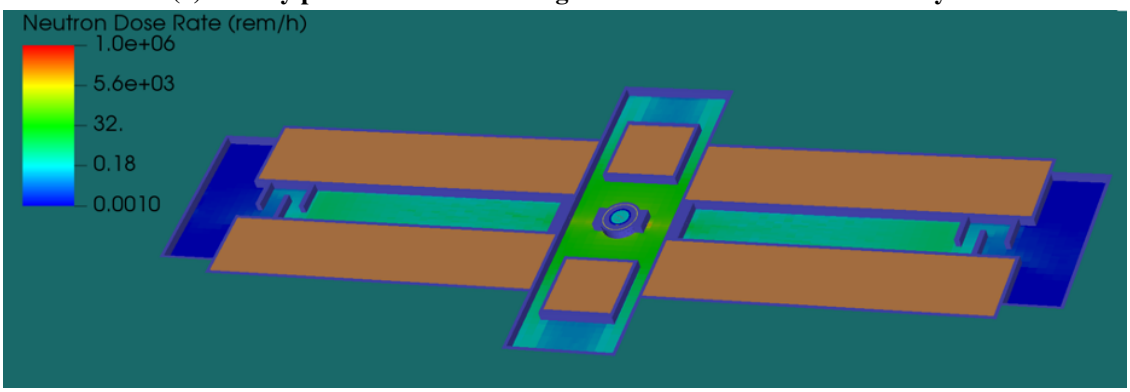

(b) Facility neutron dose rates along accelerator tunnels and walkways

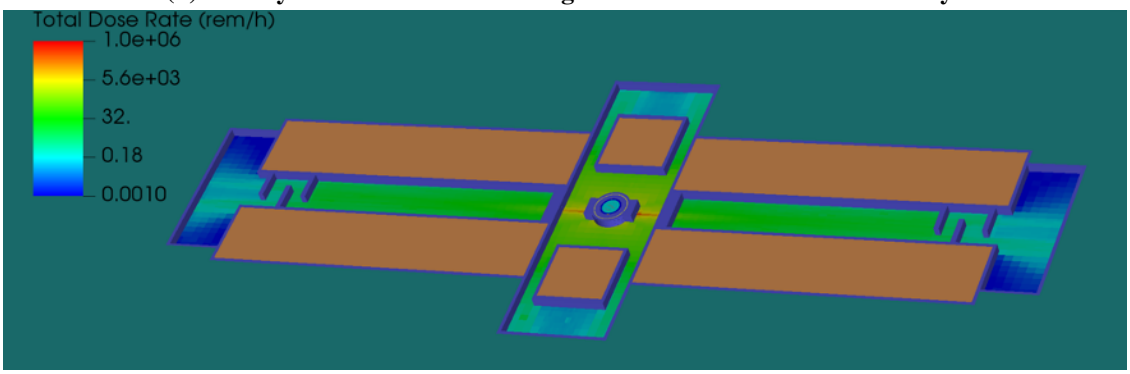

(c) Facility total dose rates along accelerator tunnels and walkways

Figure 13. Predicted core-level facility dose rates. Iteration of Niowave facility indicating areas to shield further in accelerator tunnels and perpendicular corridors without shielding.

vessel. Exclusion zones just above the UTA vessel's steel plate and at the stairways would likely maintain dose rates below the regulatory limits specified for workers at the facility.

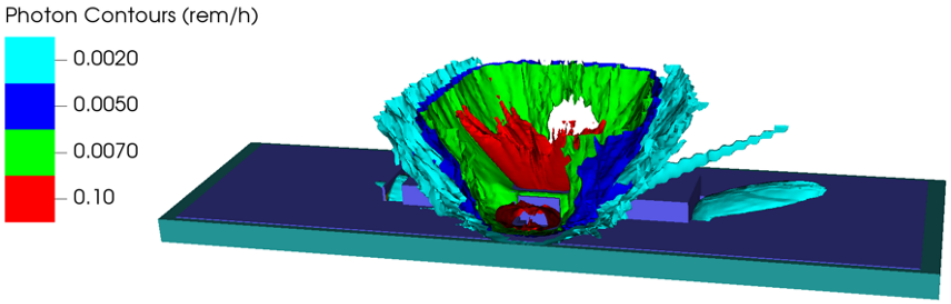

(a) UTA-3 photon dose rate contours between 2 and 100 mrem·h^{-1}

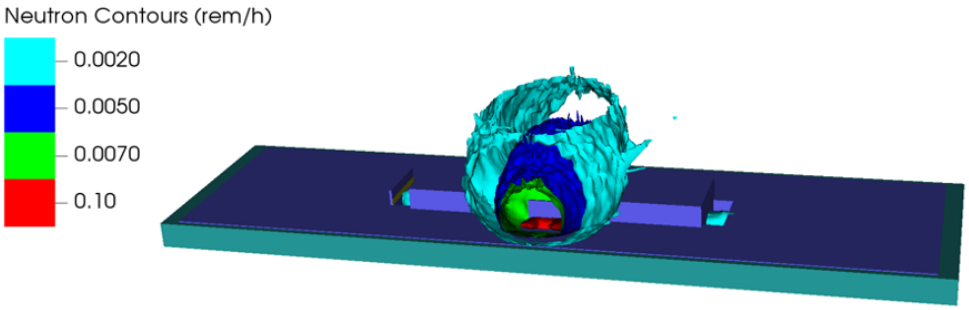

(b) UTA-3 neutron dose rate contours between 2 and 100 mrem·h^{-1}

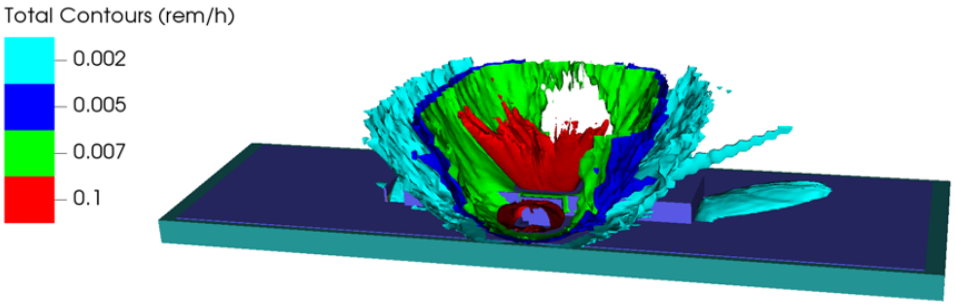

(c) UTA-3 total dose rate contours between 2 and 100 mrem·h^{-1}

Figure 14. Niowave facility indicating areas of high dose rates for neutrons and photons. Regulatory limits of 2 to 5 mrem·h^{-1} indicated that the upper personnel area above the core vessel would largely exceed regulatory limits.

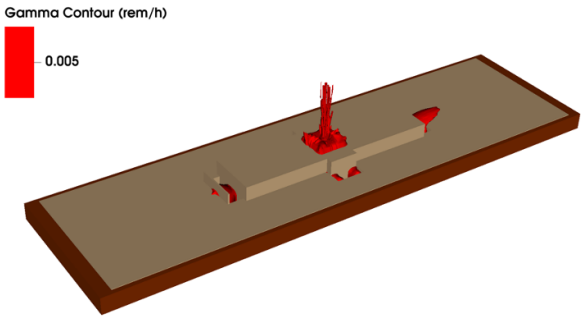

(a) UTA-3 facility photon dose rate contour at 5 mrem·h^{-1}

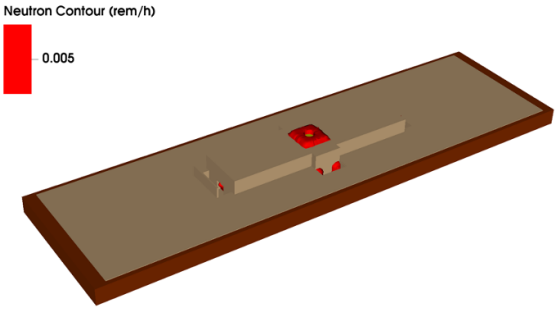

(b) UTA-3 facility neutron dose rate contour at 5 mrem·h^{-1}

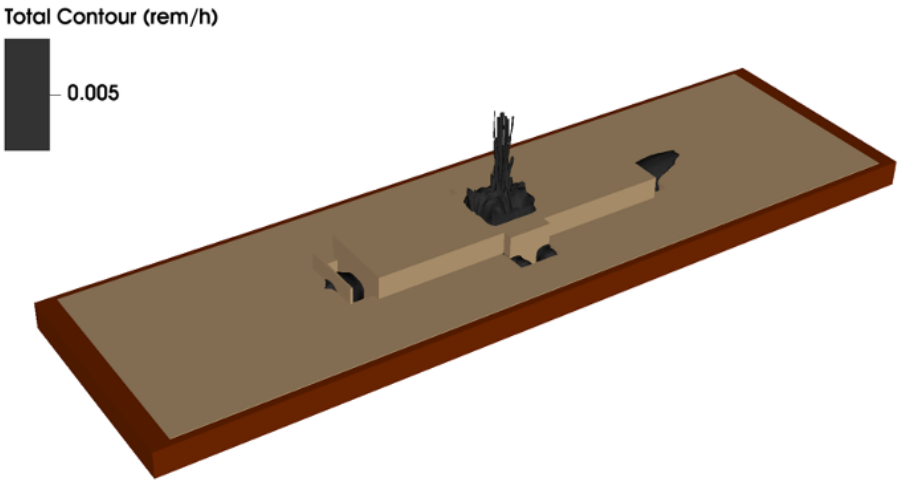

(c) UTA-3 facility total dose rate contour at 5 mrem·h^{-1}

Figure 15. Final Niowave facility dose rate contours. Dose rates dropped notably outside the Niowave UTA-3 tunnels due to increased shielding.

To better quantify the improvements of the weight window variance reduction, the Niowave full-facility model adjusted the adjoint sources to tally regions of interest. These regions include the upper tunnel wall just outside the accelerator tunnel and an upper steel trap door just above the reactor vessel. These are two far-field locations that receive little to no flux when run in analog transport. As shown in Table 1, the results between analog and optimized weight windows proved informative. Unsurprisingly, the near-field tallies produced a lower figure of merit (FOM) in the weight windows because those regions were not optimized. The LBE track-length tally for both neutrons and photons was in excellent agreement, but the FOM was higher in the analog transport. Every other tally for neutrons improved the FOM compared with the analog simulation. The difficulty of this analog and weight window problem was the lack of stats on the far-field locations. The best-defined neutron tally improved by 6×, even though the two optimized tallies were infinitely better than the analog result. The upper steel cover tally in Table 1 (a larger portion of the steel plate on top of the reactor vessel) was a nonoptimized tally but suggested a 52× improvement for photons. This improvement is largely because the adjoint source on the adjacent small steel trap door was also pushing particles through the nonoptimized tally region. An important caveat for the FOM in this work was the lack of compute resource requirements to build the weight windows. The FOM for the weight window tallies would be reduced to account for this additional compute time. Overall, the optimized tallies in this scenario were reduced to 3%–8% uncertainties, thereby highlighting the improvements that weight windows made on the facility tallies.

Table 1. Comparison of analog and weight window (WW) tallies

Tally Location	Particle Type	Analog TL[a]	Analog Rel. Err.	Analog FOM	WW TL[a]	WW Rel. Err.	WW FOM	FOM Ratio (WW / Analog)
LBE	Neutron	5.42E−2	0.0010	7.8E+0	5.40E−2	0.0016	5.8E+0	0.7
Concrete vessel	Neutron	3.30E−2	0.0020	2.1E+0	3.28E−2	0.0024	2.7E+0	1.3
Tunnel shield	Neutron	1.05E−4	0.0312	8.6E−3	1.06E−4	0.0169	5.2E−2	6.0
Upper steel cover	Neutron	—	—	—	7.35E−9	0.0148	6.8E−2	Infinite
Upper tunnel wall[b]	Neutron	—	—	—	1.60E−10	0.0450	7.4E−3	Infinite
Upper steel trap door[b]	Neutron	—	—	—	6.42E−11	0.0840	2.1E−3	Infinite
LBE	Photon	6.78E+0	0.0001	2.2E+3	6.78E+0	0.0003	2.9E+2	0.19
Concrete vessel	Photon	6.44E+0	0.0006	8.3E+1	6.43E+0	0.0009	4.4E+1	0.53
Tunnel shield	Photon	1.12E−2	0.0068	5.9E−1	1.11E−2	0.0122	2.4E−1	0.49
Upper steel cover	Photon	3.59E−7	0.1977	2.1E−4	3.42E−7	0.0374	1.1E−2	52.4
Upper tunnel wall[b]	Photon	—	—	—	1.03E−7	0.0285	1.8E−2	Infinite
Upper steel trap door[b]	Photon	—	—	—	3.88E−8	0.0347	1.2E−2	Infinite

[a]Tally location track length (TL).
[b]Region was optimized in FW-CADIS calculations for tally convergence.

4. SCALE IMPROVEMENTS FOR THE ADSR

Much of this original work involved using SCALE tools such as MAVRIC to generate weight windows to use in MCNP. At the beginning of this work, SCALE did not have the necessary high-energy photon physics in SCALE-6.2 or SCALE-6.3 found in the Niowave UTA-3 design. If most of the problem could be handled in SCALE, only a small portion of the problem—electron beam conversion into primary bremsstrahlung—would be produced with MCNP and the SPSG. In support of this work, SCALE developers added more physics capabilities to the SCALE tool suite. The most notable improvements include the additional capability to simulate photonuclear physics and TTB models, both vital parts of the Niowave radiation source. The specific details for these improvements are provided in an additional ORNL report [6], including verification and validation against MCNP for simple comparisons.

A simple ADSR loosely related to the Niowave design was created for additional verification and validation of the new capabilities in SCALE. A small LBE cuboid was placed near an array of UO_2 cylindrical rods. The LBE and UO_2 rods were suspended in a cylindrical container of water for moderation and surrounded by layers of concrete and steel. Visual renderings of the simple ADSR model are shown in Figure 16.

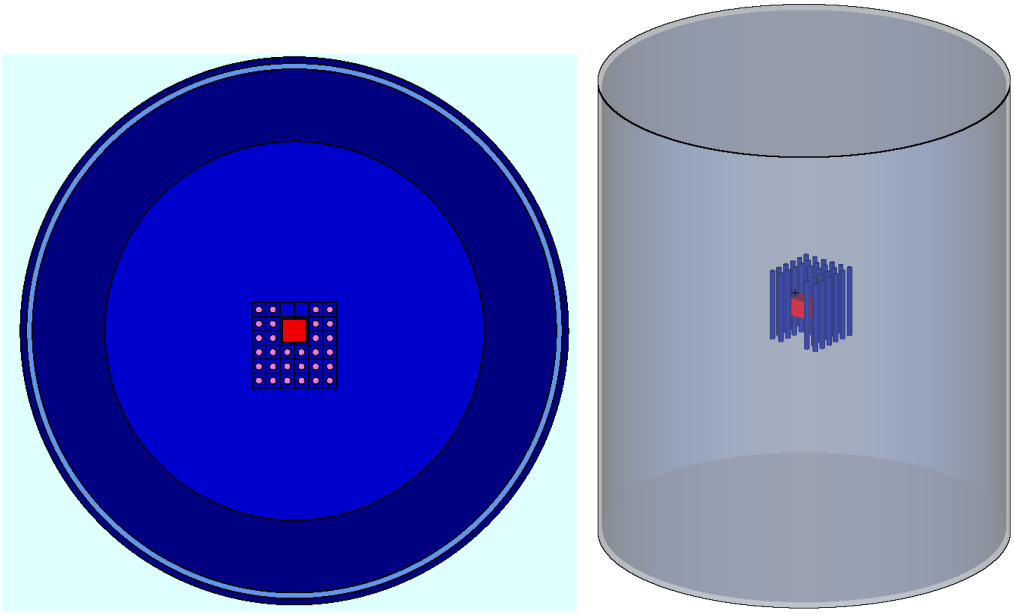

(a) Top-down cut-through of simplified ADSR model in SCALE

(b) 3D view of ADSR within a cylinder of water for moderation

Figure 16. Simplified ADSR experiment model. The ADSR example has an LBE (red) surrounded by UO_2 (pink) targets with outer fuel cladding (dark blue). Each of these materials is submersed in a water tank surrounded by concrete and steel layers.

A 40 MeV isotropic photon source was placed in the center of the LBE to create both photonuclear reactions in the LBE and the nearby UO_2. This model was designed such that criticality would not be achieved, but neutron multiplication was notable. Tallies were placed in the steel and concrete outer layers of the model to estimate the photon and neutron track lengths. A mirror model was created in MCNP for a simulation comparison between the two codes. Several versions of the model were run with new physics features

turned on and off. The simple model shares the same high-energy physics of the full-scale Niowave design, but due to its simplicity and relatively small size, the model did not require variance reduction methods such as FW-CADIS. MC transport was performed in MCNP-6.2 and a SCALE-7 beta branch with the new features. Table 2 shows four configurations comparing MCNP and SCALE, including a reference MCNP transport model with electron physics instead of TTB. Statistical uncertainty was kept below 1.5% for photon tallies, so result differences above 3%–5% may suggest transport differences between the two codes. Neutron tally uncertainties were kept below 2% uncertainty.

Table 2. Comparison of new SCALE TTB model and photonuclear (PN) physics for ADSR

Scenario	PN Physics	TTB	Fission	Electron Transport	Tally Region	Tally Particle	MCNP TL[a]	SCALE TL[a]	Pct. Diff. (%)[b]
Base (40 MeV photon)	—	—	—	—	Steel	Photon	1.57E−3	1.55E−3	−1.5
Base (40 MeV photon)	—	—	—	—	Concrete	Photon	5.59E−4	5.52E−1	−1.2
Base (40 MeV photon)	—	—	—	—	Steel	Neutron	0.0	0.0	—
Base (40 MeV photon)	—	—	—	—	Concrete	Neutron	0.0	0.0	—
Base+TTB	—	TTB	—	—	Steel	Photon	3.61E−2	3.13E−2	−13.5
Base+TTB	—	TTB	—	—	Concrete	Photon	2.34E−2	1.99E−2	−15.1
Base+TTB	—	TTB	—	—	Steel	Neutron	0.0	0.0	—
Base+TTB	—	TTB	—	—	Concrete	Neutron	0.0	0.0	—
Base+PN	PN	—	—	—	Steel	Photon	1.72E−3	1.70E−3	−1.1
Base+PN	PN	—	—	—	Concrete	Photon	6.38E−4	6.38E−4	0.0
Base+PN	PN	—	—	—	Steel	Neutron	4.43E−5	4.42E−5	−0.2
Base+PN	PN	—	—	—	Concrete	Neutron	2.55E−5	2.55E−5	0.1
Base+TTB+PN+fiss.	PN	TTB	Fission	—	Steel	Photon	3.61E−2	3.13E−2	−13.3
Base+TTB+PN+fiss.	PN	TTB	Fission	—	Concrete	Photon	2.32E−2	1.97E−2	−15.0
Base+TTB+PN+fiss.	PN	TTB	Fission	—	Steel	Neutron	2.21E−4	1.98E−4	−10.3
Base+TTB+PN+fiss.	PN	TTB	Fission	—	Concrete	Neutron	1.24E−4	1.13E−4	−9.1
Base+elec.+PN+fiss.	PN	—	Fission	Electron	Steel	Photon	3.87E−2	—	—
Base+elec.+PN+fiss.	PN	—	Fission	Electron	Concrete	Photon	2.14E−2	—	—
Base+elec.+PN+fiss.	PN	—	Fission	Electron	Steel	Neutron	2.52E−4	—	—
Base+elec.+PN+fiss.	PN	—	Fission	Electron	Concrete	Neutron	1.40E−4	—	—

[a] Track length (TL) for tally location.

[b] Percent difference uses the equation format $[(SCALE - MCNP)/MCNP * 100]$.

The "base" case in Table 2 was a 40 MeV photon source without TTB, photonuclear physics, or electron physics. This was the simplest nonphysical case to compare the two codes. Unsurprisingly, the neutron tallies of the base case produced no neutrons results, but the photon tallies were within 1.5% of each other. Statistical variation was in line with these results, so the agreement was considered adequate. In the second scenario, "base+TTB," only the TTB model was turned on in MCNP and SCALE. The results for both codes increased by more than an order of magnitude, highlighting the importance of a TTB model or electron physics in high-energy problems such as the Niowave design. In this scenario, the results were approximately 13%–15% lower for the new SCALE TTB model versus MCNP. Because the MC statistical uncertainties were below 1% in this test case, the methods were producing different results. Scenario 3, "base+PN," removed the TTB and turned on the photonuclear physics. This result was run to low uncertainties, and the neutron and photon tallies matched to ∼1%, showing excellent agreement without the TTB model. Scenario 4, "base+TTB+PN+fiss.," melds all the physics, including fission production in the UO_2 rods. As with scenario 2, the photon tallies in SCALE are 13%–15% lower than MCNP, even with photon tally uncertainties below 1%. The neutron fluxes were within 9%–10% between both codes. The neutron tallies were both outside statistical uncertainty. A plausible reason for the discrepancy in neutron tallies was that fewer high-energy photons were produced, which could be implied by the photon tally results also being lower than those of MCNP. This simple test case was instructive for the Niowave design and other ADSRs, but it

was not a full representation of the physics between the two codes. For example, this work did not explore the differences in photon spectra across each tally nor a vast array of nuclides, so a user's results may show better or worse agreement when using response-weighted tallies or other problem-specific nuclides.

4.1 NIOWAVE UTA-3 WITH BREMSSTRAHLUNG SOURCE

To convey the full abilities of SCALE's new photonuclear and bremsstrahlung physics, the team simulated the full-scale Niowave model of the UTA-3 facility using only the reduced-order bremsstrahlung source in SCALE. This approach required using the SPSG to create a photon source from the electron beam in MCNP, but the remaining transport outside the LBE was performed in SCALE using the new physics capabilities created for this work. Additionally, the MAVRIC variance reduction features were used to combine the complex physics and necessary variance reduction features highlighted in this report. MCNP simulated the same reduced-order bremsstrahlung source with TTB models and the same weight windows as used in the SCALE mesh importance map file. This work did not attempt to estimate the FOM differences between the codes.

As seen in Table 3, the results are largely in good agreement for the full-scale Niowave model with some caveats. The near-field tallies such as the LBE and concrete core vessel matched to within 4%. All but one neutron tally matched to within 5% between the codes. One tally was 60% higher in SCALE than MCNP. This is most likely due to high-weight, low-energy particles interacting in the concrete core vessel within SCALE; MCNP roulette did not allow similar particles to reach the concrete vessel. Excluding tally 24, the tallies are in good agreement between MCNP and SCALE. Based on good agreement between the two codes, SCALE could be a viable option for MC radiation transport using the additional capabilities implemented during this work.

Table 3. SCALE and MCNP tracklength estimation for the Niowave UTA-3 with a bremsstrahlung source

Description	Tally Number	Particle Type	MCNP		SCALE		SCALE / MCNP
			TL[a]	Rel. Err.	TL[a]	Rel. Err.	
LBE	4	Photon	5.17E+17	0.0000	5.08E+17	0.0001	0.98
Concrete core vessel[b]	14	Photon	5.34E+17	0.0183	8.56E+17	0.3131	1.60
Concrete tunnel shield	24	Photon	1.13E+15	0.0305	9.88E+14	0.0594	0.87
End of tunnel wall	34	Photon	9.13E+9	0.0163	8.44E+9	0.0177	0.92
Steel door above vessel	44	Photon	2.30E+9	0.0358	2.08E+9	0.0268	0.91
LBE	104	Neutron	3.67E+15	0.0014	3.59E+15	0.0024	0.98
Concrete core vessel	114	Neutron	2.26E+15	0.0044	2.18E+15	0.0085	0.96
Concrete tunnel shield	124	Neutron	7.12E+12	0.0154	6.76E+12	0.0283	0.95
End of tunnel wall	134	Neutron	1.05E+7	0.0366	8.16E+16	0.0374	0.78
Steel door above vessel	144	Neutron	4.16E+6	0.0874	3.93E+6	0.0562	0.95

[a] Track length (TL) was estimated with both tools using volumes set to 1.0 cm^3 for consistency.

[b] SCALE analysis shows extremely high error in the photon 10–100 keV energy bin, which also has the most TL. Because the source was not biased, this spike in TL is likely from a few high-weight particles reaching the concrete vessel that MCNP did not register.

5. CONCLUSIONS AND FUTURE WORK

Radiation shielding is a challenge for complex systems with high-energy particles such as Niowave's proposed ADSR. Based on the results produced from this work, the weight window variance reduction method can produce effective results for accelerator-driven systems such as Niowave's ADSR. There was a dramatic improvement to dose response statistics outside the facility tunnels where personnel were expected. The dose response weighting was found to be beneficial in focusing both photons and neutrons toward regions of interest. However, some nonoptimized tallies were worse within the core region, so core region analysis can likely continue to leverage analog transport or should apply additional tally optimization to all tallies. Comparison between analog and weight window simulations indicated tally speedups of 50× or more. Based on the optimization methods described in this report, Niowave can use contour plots of the 3D dose map to determine areas of concern within the facility. Additionally, the new SCALE photonuclear and TTB capabilities greatly improve the capabilities of SCALE for accelerator-driven systems and demonstrate good agreement with MCNP.

Because most of the weight window tally results agreed with analog transport results and improved FOM at far-field locations, the methodology to generate the weight windows remains a valid option for ADSR dose modeling. The combination of a SPSG source inside the MAVRIC and Denovo framework can generate reasonable importance maps.

The Denovo deterministic transport lacked fission source production and exhibited issues with an anisotropic source. Improvements to the Denovo deterministic transport code could improve the adjoint solution and remove the need to tweak weight windows with a code such as Frankenstein or other clever optimization methods. Furthermore, if photonuclear multigroup cross sections are implemented into Denovo, no need would exist to create a photoneutron source because the production pathway would be accounted for in Denovo. If variance reduction methods can employ the photonuclear cross sections, anisotropic source sampling, and handle fission production, the stand-alone CADIS method might be fully sufficient for complex systems such as the Niowave design. Even without these improvements, the methods discussed proved sufficient for the Niowave design and should be considered for radiation dose modeling in similar systems. Finally, one could further investigate the use of a deterministic solution as a preconditioner to the MCNP weight window generator method to capture the full physics found in complex systems such as the Niowave design.

6. REFERENCES

[1] T E Booth and J S Hendricks. "Importance estimation in forward Monte Carlo calculations". In: *Nucl. Technol./Fusion; (United States)* 5 (Jan. 1984). URL: https://www.osti.gov/biblio/6189406.

[2] Hank Childs et al. *High Performance Visualization–Enabling Extreme-Scale Scientific Insight*. 2012. DOI: 10.1201/b12985. URL: https://visit.llnl.gov.

[3] Thomas Evans et al. "Denovo–A New Three-Dimensional Parallel Discrete Ordinates Code in SCALE". In: *Nuclear Technology - NUCL TECHNOL* 171 (Aug. 2010), pp. 171–200. DOI: 10.13182/NT171-171.

[4] T Heltemes, P Karcz, and J Dix. "Ensuring a stable supply of Mo-99 in the United States without the use of HEU". In: *Proc. ICONS-2020* (2020), pp. 10–14.

[5] Domen Kotnik et al. "Validation and evaluation of the ADVANTG hybrid code on the ICSBEP labyrinth benchmark experiment". In: *Annals of Nuclear Energy* 114 (2018), pp. 464–481. ISSN: 0306-4549. DOI: https://doi.org/10.1016/j.anucene.2017.12.011. URL: https://www.sciencedirect.com/science/article/pii/S0306454917304620.

[6] Robert Alexander Lefebvre et al. "Photonuclear Physics in SCALE". In: (Jan. 2024). DOI: 10.2172/2282948. URL: https://www.osti.gov/biblio/2282948.

[7] Scott W. Mosher et al. "ADVANTG An Automated Variance Reduction Parameter Generator, Rev. 1". In: (Aug. 2015). DOI: 10.2172/1210162. URL: https://www.osti.gov/biblio/1210162.

[8] Noel B. Nelson et al. "Radiation Shielding Analysis of Niowave's Uranium Target Assembly 2 (UTA-2) Facility for Molybdenum-99 Production". In: (July 2022). DOI: 10.2172/1878714. URL: https://www.osti.gov/biblio/1878714.

[9] Douglas E. Peplow. "Monte Carlo Shielding Analysis Capabilities with MAVRIC". In: *Nuclear Technology* 174.2 (Jan. 2011). ISSN: 0029-5450. DOI: 10.13182/NT174-289. URL: https://www.osti.gov/biblio/1017290.

[10] Michael Evan Rising et al. *MCNP® Code Version 6.3.0 Release Notes*. Tech. rep. LA-UR-22-33103, Rev. 1. Los Alamos, NM, USA: Los Alamos National Laboratory, Jan. 2023. DOI: 10.2172/1909545. URL: https://www.osti.gov/biblio/1909545.

[11] X-5 Monte Carlo Team. "MCNP - Version 5, Vol. I: Overview and Theory". In: (2003).

[12] John C Wagner and Scott W Mosher. "Forward-Weighted CADIS Method for Variance Reduction of Monte Carlo Reactor Analyses". In: (Jan. 2010). URL: https://www.osti.gov/biblio/992539.

[13] John C Wagner, Douglas E Peplow, and Scott W Mosher. "FW-CADIS Method for Global and Regional Variance Reduction of Monte Carlo Radiation Transport Calculations". In: *Nuclear Science and Engineering* 176 (1 Jan. 2014). doi: 10.13182/NSE12-33, pp. 37–57. ISSN: 0029-5639. DOI: 10.13182/NSE12-33. URL: https://doi.org/10.13182/NSE12-33.

[14] John C. Wagner and Alireza Haghighat. "Automated Variance Reduction of Monte Carlo Shielding Calculations Using the Discrete Ordinates Adjoint Function". In: *Nuclear Science and Engineering* 128.2 (1998), pp. 186–208. DOI: 10.13182/NSE98-2. eprint: https://doi.org/10.13182/NSE98-2. URL: https://doi.org/10.13182/NSE98-2.

[15] Christopher John Werner et al. "MCNP Version 6.2 Release Notes". In: (Feb. 2018). DOI: 10.2172/1419730. URL: https://www.osti.gov/biblio/1419730.

[16] William Wieselquist and Robert Alexander Lefebvre. "SCALE 6.3.1 User Manual". In: (Feb. 2023). DOI: 10.2172/1959594. URL: https://www.osti.gov/biblio/1959594.